ACSNANO

www.acsnano.org

ARTICLE

Aptamer Nanoconstructs Crossing Human Blood–Brain Barrier Discovered via Microphysiological System-Based SELEX Technology

Jeong-Won Choi,[▽] Minwook Seo,[▽] Kyunghwan Kim, A-Ru Kim, Hakmin Lee, Hyung-Seok Kim, Chun Gwon Park, Seung Woo Cho, Joo H. Kang, Jinmyoung Joo,* and Tae-Eun Park*

Cite This: https://doi.org/10.1021/acsnano.2c11675

Read Online

ACCESS | Metrics & More | Article Recommendations | Supporting Information

Downloaded via Tae-Eun Park on April 18, 2023 at 00:55:35 (UTC).
See https://pubs.acs.org/sharingguidelines for options on how to legitimately share published articles.

ABSTRACT: Blood–brain barrier (BBB) remains one of the critical challenges in developing neurological therapeutics. Short single-stranded DNA/RNA nucleotides forming a three-dimensional structure, called aptamers, have received increasing attention as BBB shuttles for efficient brain drug delivery owing to their practical advantages over Trojan horse antibodies or peptides. Aptamers are typically obtained by combinatorial chemical technology, termed Systemic Evolution of Ligands by EXponential Enrichment (SELEX), against purified targets, living cells, or animal models. However, identifying reliable BBB-penetrating aptamers that perform efficiently under human physiological conditions has been challenging because of the poor physiological relevance in the conventional SELEX process. Here, we report a human BBB shuttle aptamer (hBS) identified using a human microphysiological system (MPS)-based SELEX (MPS-SELEX) method. A two-channel MPS lined with human brain microvascular endothelial cells (BMECs) interfaced with astrocytes and pericytes, recapitulating high-level barrier function of *in vivo* BBB, was exploited as a screening platform. The MPS-SELEX procedure enabled robust function-based screening of the hBS candidates, which was not achievable in traditional *in vitro* BBB models. The identified aptamer (hBS01) through five-round of MPS-SELEX exhibited high capability to transport protein cargoes across the human BBB via clathrin-mediated endocytosis and enhanced uptake efficiency in BMECs and brain cells. The enhanced targeting specificity of hBS01 was further validated both *in vitro* and *in vivo*, confirming its powerful brain accumulation efficiency. These findings demonstrate that MPS-SELEX has potential in the discovery of aptamers with high target specificity that can be widely utilized to boost the development of drug delivery strategies.

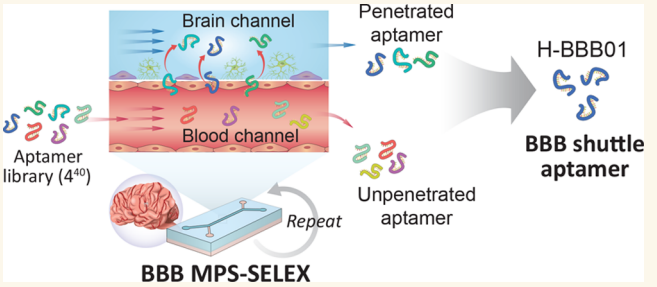

KEYWORDS: *blood–brain barrier, SELEX, microphysiological system, BBB shuttle aptamer, brain drug delivery*

INTRODUCTION

The blood–brain barrier (BBB) is a term used to describe the selective barrier properties of the microvasculature of the central nervous system (CNS). The BBB is formed by a lining of brain microvascular endothelial cells (BMECs), its underlying basement membrane, pericytes, and astrocytes.[1] Although the properties of the BBB are largely manifested within BMECs, critical interactions with surrounding cells and the extracellular matrix create a heavily restricting barrier capacity, which tightly regulates CNS homeostasis. The property of very low paracellular permeability is controlled by tight junction complexes between the BMECs, restricting the entry of molecules between blood and the brain.[1] Therefore, the human BBB poses a difficult challenge for brain-targeted drug delivery, preventing the transport of approximately 100% of large (>500 Da) molecules into the brain.[2]

Several strategies aim to overcome this obstacle and promote efficient and specific crossing of therapeutically relevant agents across the BBB. One such strategy uses the

Received: November 23, 2022
Accepted: April 3, 2023

© XXXX American Chemical Society

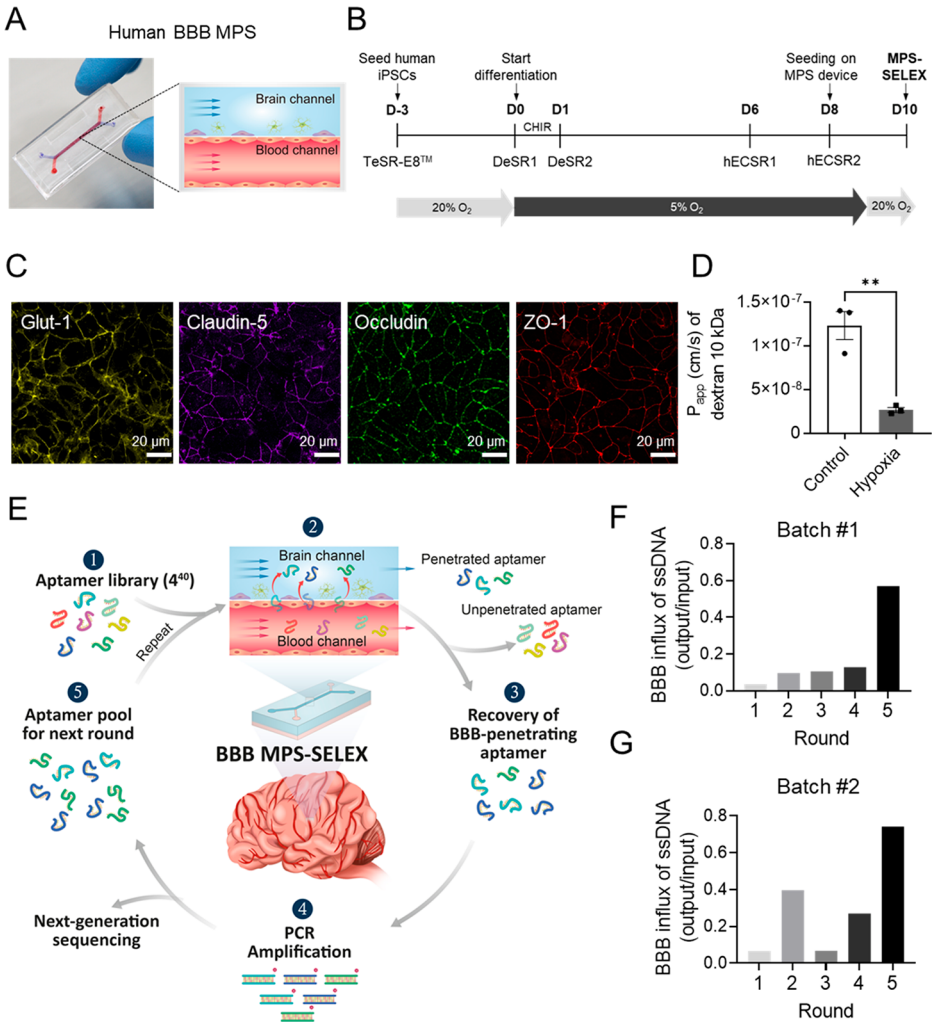

Figure 1. Reconstruction of the BBB MPS and MPS-SELEX approach to identify BBB penetrating aptamers. (A) The photograph of the fabricated BBB MPS device (left panel) and the scheme of the structure of BBB MPS (right panel). The iPS-BMECs are cultured on all surfaces of the basal vascular channel, whereas primary astrocytes and pericytes are cocultured on the upper surface of the PET membrane in the apical brain channel. (B) Timeline for the differentiation of the human iPS-BMECs under hypoxic stimuli, seeding in the MPS device, and performing MPS-SELEX. (C) Immunofluorescence micrographs of iPS-BMECs in the BBB MPS labeled with Glut-1, Cluadin-5, Occludin, and ZO-1. (D) Permeability coefficient of the BBB MPS cultured under normoxic (control) and hypoxic (hypoxia) conditions. For statistical analysis, an unpaired *t* test was performed. ($P < 0.01$). (E) Schematic diagram of MPS-SELEX process. The starting ssDNA library or the PCR-amplified pool from previous selection either flowed into the blood channel of the BBB MPS, and BBB permeable ssDNA is collected from brain channel efflux. The sequences of collected ssDNA at 5th round of SELEX are obtained using NGS. (F) The w/w ratio of output/input aptamers across the BBB in the first batch of MPS-SELEX. (G) The w/w ratio of output/input aptamers across the BBB in the second batch of MPS-SELEX.**

physiological process of receptor-mediated transcytosis (RMT) to transport cargo across the BBB, which is less limited by the size and shape constraints of carrier-mediated transports.[2] Advances in our understanding of intracellular trafficking and receptor binding, as well as in protein engineering and nanotechnology, have enabled the delivery of CNS therapeutics using RMT.[3] Thus, a variety of brain shuttles, mostly monoclonal antibodies against receptors (e.g., transferrin receptor and insulin receptors) expressed on the brain endothelium, have been widely investigated, and conjugation of these antibodies to drugs or nanoparticles has become a mainstream approach for brain drug delivery approach.[4,5] In addition, BBB-shuttling peptides, including Angiopep-2,[6] THR,[7] and TGN,[8] have proven useful in delivering cargo to the CNS using RMT. However, aptamers serving as oligonucleotide ligands by folding in a tridimensional structure have been suggested to offer an attractive alternative owing to their practical advantages over antibodies or peptides, including lower cost, smaller size, reduced immunogenicity, and higher chemical and biological versatility.[9] Because of the promising potential of aptamers as BBB shuttles, tremendous efforts have been made to identify aptamers that selectively deliver drugs into the CNS.[10−13] However, most sequences obtained from conventional methods of aptamer selection showed nonspecific or poor performance, hindering their practical applications in brain drug delivery.

Currently, aptamers are selected using the Systematic Evolution of Ligands by EXponential enrichment (SELEX) methodology developed by Tuerk[14] and Ellington.[15] This procedure is based on the isolation of high-affinity ligands from a combinatorial single-stranded nucleic acid library through repeated cycles of binding, partitioning, and amplification.[16]

https://doi.org/10.1021/acsnano.2c11675
ACS Nano XXXX, XXX, XXX−XXX

Following SELEX cycles, the final aptamer pool is subjected to sequencing to identify the best binding sequences providing the required function.[17] Traditionally, the SELEX method was performed based on the knowledge of the target for aptamer selection. For brain drug delivery, aptamers binding to the purified transferrin receptor (TfR) have often been identified as BBB shuttle oligonucleotides in previous studies.[10,11] However, the main drawback of traditional SELEX is that the selected aptamers do not specifically target proteins in their native states (in the cells).[12] To overcome this issue, an *in vivo* evolution strategy has been employed to select aptamers with enhanced penetration into the brain when injected systemically into a living mouse. Through 22 rounds of *in vivo* selection, a previous study identified an aptamer exhibiting high BBB penetration capacity.[13] This approach can ensure the capacity of the aptamer to cross over the BBB under physiological conditions;[13] however, species differences of BBB between mouse and human hinder the selection of aptamers targeting human BBB.[18] To identify aptamers that perform efficiently under human physiological conditions, cell-SELEX using an *in vitro* human BBB model has been suggested as an optimal approach. Despite the unquestionable advantages of cell-SELEX, this method cannot be widely applied to discover a BBB shuttle[19] because of the poor physiological relevance of the *in vitro* cultures of primary or immortalized human BMECs. Dua et al. reported the aptamer with human and mouse cross-reactivity using combination of human and mouse cell-SELEX.[20] However, they utilized the hCMEC/D3 immortalized cell line on a 2D culture dish as a screening platform, which only enables screening of internalized aptamers, not penetrated aptamer. As such, paracellular leakage occurring in the past *in vitro* BBB models limited the robust screening of small-sized oligonucleotides with a strong BBB shuttling capacity. Given that the similarity of the BBB platform to the human BBB may determine the success of cell-SELEX, in this study, we employed a microphysiological system (MPS) technology for successful identification of human BBB shuttle.

Considering the rapid development in MPSs and stem cell technologies, we previously developed a microfluidic BBB MPS model lined with induced pluripotent stem cell (iPSC)-derived human BMECs (iPS-BMECs) interfaced with primary human brain astrocytes and pericytes that recapitulate the high-level barrier function of the *in vivo* human BBB.[21] Increased barrier functionality was accomplished using a developmentally inspired induction protocol that includes a period of differentiation under hypoxic conditions[21] and physiological flow. Importantly, we demonstrated that the BBB endothelium displays selective transcytosis of peptides and antibodies and a highly active efflux pump under optimized fluid flow, implying its potential as a reliable BBB shuttle screening tool.[21] Building on this success, we hypothesized that SELEX approach based on a human MPS (MPS-SELEX) could be a promising strategy to identify aptamers with human BBB shuttling capacity under physiological conditions.

In this study, MPS-SELEX was performed using a human BBB MPS system to identify single-stranded DNA aptamers with BBB shuttling capacity, without disrupting barrier function. After investigating the top-ranked aptamers using next-generation sequencing, their BBB shuttling efficiencies were compared in human BBB MPS and human brain slices, and the best-validated sequence (hBS01) was selected. The vascular bed-specific targeting of hBS01 was confirmed by validating its shuttling capacity between the vascular endothelium of the brain and other organs. Moreover, through a series of inhibitory experiments, we found that the BBB shuttling capacity of hBS01 was associated with clathrin-mediated transport, as shown in many other BBB shuttle molecules. The *in vivo* BBB shuttling potency of hBS01 was further validated in mice, confirming its powerful brain accumulation efficiency. This suggests that MPS-SELEX could be useful in the discovery of a human BBB shuttle aptamer that is strongly active *in vitro* and *in vivo*.

RESULTS AND DISCUSSION

MPS-SELEX Approach to Identify BBB Penetrating Aptamers. To select aptamers that can recognize human BMEC and penetrate the BBB under physiological conditions, we developed a MPS-SELEX, which uses human BBB MPS as a complex target for aptamer selection. Our previously developed human BBB MPS was reconstituted in a poly(dimethylsiloxane) (PDMS) device containing an upper brain channel and a lower blood channel separated by a highly permeable polyester terephthalate (PET) membrane (2 μm pore). The blood channel is lined with human iPS-BMECs interfaced with a brain channel where human primary astrocytes and pericytes are cultured (Figure 1A). The transport of treated drugs from the brain endothelium to the brain can be efficiently predicted using human BBB MPS by analyzing the effluent obtained from each microchannel. In particular, this fully perfusable two-channel platform without hydrogel filling is ideal for harvesting BBB-permeable aptamers during the MPS-SELEX procedure.

The BBB MPS used in the current study was fabricated using human iPS-BMECs generated by direct differentiation of iPSC to accelerate their endothelial cell fate,[22] while our previous platform was established using iPS-BMECs obtained by the neural and endothelial progenitor codifferentiation method.[21,24] Furthermore, to enhance the BBB attributes of iPS-BMECs, iPSCs were differentiated under exposure to hypoxic stimuli, as previously demonstrated (Figure 1B).[21] Hypoxia stimuli-enhanced iPS-BMECs exhibited a higher and more stable endothelial barrier function, in agreement with our previous report when trans-endothelial electrical resistance was monitored (Supplementary Figure 1A). The BBB cultured under hypoxic condition displayed BBB marker gene expression such as junction, receptor, and solute carrier protein, but higher gene expression level of one of the efflux pump proteins (ABCC2) compared to control (Supplementary Figure 1B,C). Confocal immunofluorescence microscopic analysis after 2 days of culture on an MPS device revealed that the iPS-BMEC monolayer was formed in the microvessel channel (Figure 1C). The iPS-BMEC monolayer showed the expression of junctional complexes containing ZO-1, Claudin-5, and occludin and glucose transporter 1 (GLUT-1). The paracellular permeability of the BBB MPS to dextran 10 kDa was very low (2.5×10^{-8} cm/s), as shown in our previous study,[21] confirming that human BBB MPS can recapitulate the barrier function of *in vivo* BBB[25] (Figure 1D).

Next, we used this physiologically relevant human BBB-MPS to select BBB-penetrating aptamers (Figure 1E). The MPS-SELEX procedure consists of three major steps: (1) dosing of the single-stranded DNAs (ssDNA) library through the vascular channel under fluid flow, (2) collecting the BBB penetrating ssDNA from the brain channel effluent, and (3)

https://doi.org/10.1021/acsnano.2c11675
ACS Nano XXXX, XXX, XXX−XXX

A

Name	Sequence	Ranking	
		Batch #1	Batch #2
hBS01	GTCGGTAGCCACTCTGCGTTGTCTATAAGTTACCGTATCT	1	2
hBS02	GCCGTGTGCTGCCACTGCCAAACTCATTCGATCACACTGA	2	4
hBS03	TACCACACATGCACGACTGGAATCTTCCCCCCCTGAATGG	3	3
hBS04	ACCTCCCTTATCGACCATTGAATAGTTCCCTCTCTCTGTTGA	4	1
hBS05	TTGGGCAGTATTACACGTACTACGCGAGGCAATGCAACGTA	6	6
hBS06	GTCCAACAGCACTTACGAATCATACTACTGCTCTATCGCT	7	5

B

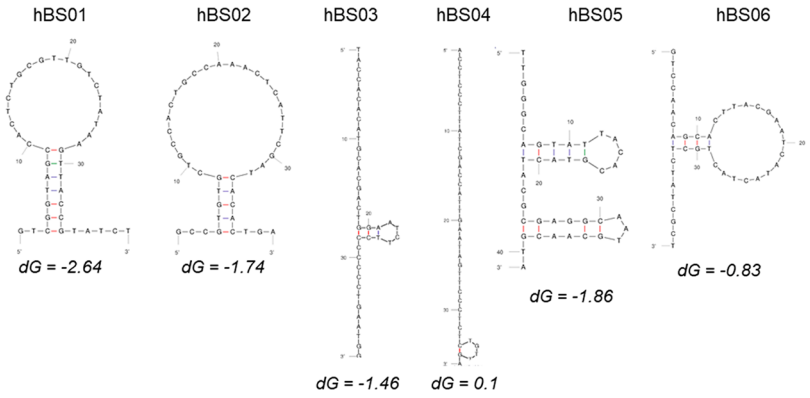

Figure 2. Sequences of aptamers obtained by NGS analysis of ssDNA after five rounds of MPS-SELEX. (A) The top six ranked human BBB shuttling aptamers (hBS) discovered from first and repeated batch of MPS-SELEX. (B) The secondary structure of selected aptamers simulated by the M-fold software. *dG* = Gibbs free energy.

amplification of the ssDNA pool for the next round by polymerase chain reaction (PCR), as schematized in Figure 1E. The ssDNA library used in this study was based on the method described by Ouellet et al.[26] with some modifications. The ssDNAs was composed of a 40-mer core region, flanked by a 25-mer and 20-mer sequence at the 5′ and 3′ end, respectively, for primer binding (Supplementary Figure 2). The designed sequences aimed to enhance the stability of the aptamer structure and minimize any potential interference between the flanking and core regions. This strategy facilitated the binding of the aptamer to target molecules during the SELEX process. The 3′-block was biotinylated to efficiently isolate aptamers using a biotin-avidin reaction. The stability of primer site hybridization during screening was confirmed by incubating aptamers in medium up to 24 h (Supplementary Figure 3). Optimized flow conditions may be critical for successful aptamer selection in MPS. We found that a high flow rate (1 mL/h) reduced the chance of aptamer binding to the iPS-BMEC, disabling the recovery of transported aptamers for the next round of SELEX. Because we successfully recapitulated BBB-shuttling activities with a flow rate of 100 μL/h in our previous work,[21] the same flow conditions were used during the MPS-SELEX. In total, five rounds of SELEX were performed in an MPS, progressively increasing the selection pressure by changing the dose of treated ssDNA library (Table S1); these procedures were repeated once more to validate whether MPS-SELEX can provide consistent screening results. Following each round, we monitored the ratio of BBB-penetrating aptamers and the maintenance of barrier integrity during SELEX by analyzing the permeability of lucifer yellow as a tracer.

PCR analysis of recovered aptamers at each round revealed enhanced BBB penetration by rounds of SELEX, showing 15- (batch 1) and 11.5-times (batch 2) greater extent of aptamers recovered from the brain microchannel after fifth round of SELEX compared to the first round (Figure 1F,G). Paracellular transport of lucifer yellow maintained its constant level during five rounds of MPS-SELEX (Supplementary Figure 4), ensuring that multiple rounds of MPS-SELEX enriched the aptamers with BBB penetrating capacity without disrupting the barrier integrity of human BBB MPS. These data suggest that BBB-penetrating aptamers can be successfully enriched in as few as five rounds, which proves the robustness of MPS-SELEX compared to the previous *in vivo* SELEX study that required 28 rounds of selection.[13] To isolate aptamers with high BBB penetration capacity, the aptamer recovered from the brain channel was sequenced after fifth round of MPS-SELEX (Figure 1E). The sequencing of the aptamer pool revealed the six most enriched aptamers (hBS01−hBS06). The top sequences were almost identical between the two batches of MPS-SELEX, demonstrating that MPS-SELEX using the human BBB MPS provides a reliable and repeatable screening method (Figure 2A). When predicting their secondary structures using the M-fold web server,[27] we could not identify common structural features among the six self-hybridized aptamers (Figure 2B). However, hBS01, hBS02, hBS05, and hBS06 have the potential to form stem-loop structures, which may play a fundamental role in target molecule bindings.

***In Vitro* Assessment of BBB Penetration of Aptamer Candidates.** Next, we validated the BBB-penetrating capacity of the top-ranked aptamers using both the BBB transwell model and BBB MPS to identify the most promising BBB shuttle. First, the BBB permeability of the top six chemically synthesized aptamers was tested using a BBB transwell model. It revealed that hBS01, hBS04, and hBS06 had more than 2-fold higher BBB penetration capacity than the starting pool (ssDNA library), whereas hBS02, hBS03, and hBS05 did not show greater BBB permeability (Figure 3A). No significant

https://doi.org/10.1021/acsnano.2c11675
ACS Nano XXXX, XXX, XXX−XXX

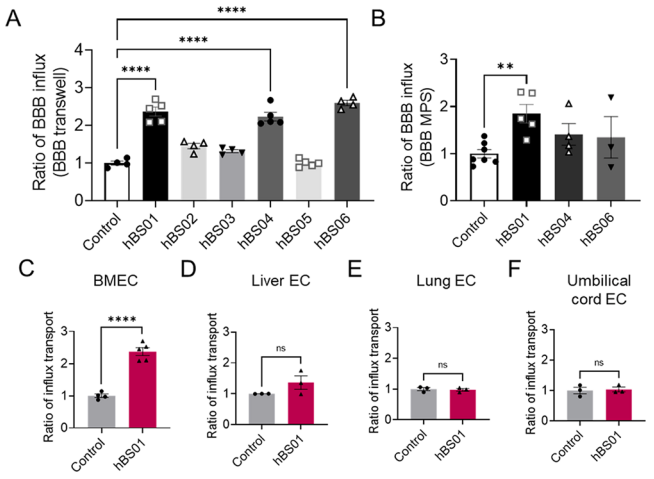

Figure 3. Verification of BBB penetrating efficacy and enhanced brain specificity of aptamer candidates. (A) BBB penetration efficiencies of aptamers identified through MPS-SELEX versus starting pool (control) in the human BBB transwell model and (B) the BBB MPS. Ratio of BBB penetration efficacy of hBS01 versus starting pool in endothelial transwell models consisting of (C) iPSC-BMECs, (D) liver, (E) lung, and (F) umbilical cord endothelial cells. For statistical analysis, an unpaired *t* test was performed. ($P < 0.01$; ****$P < 0.0001$).**

changes in trans-endothelial electrical resistance (TEER; ~3000 Ω × cm^2) were detected in the iPS-BMEC monolayer after incubation with these BBB shuttle candidates (Supplementary Figure 5), indicating aptamer candidates cross over the BBB without damaging the barrier. After narrowing down the potential candidates, we tested the BBB penetration capacity of hBS01, hBS04, and hBS06 using human BBB MPS. Among the three aptamers, only hBS01 showed a significantly higher BBB penetration capacity compared to the starting pool, whereas hBS04 and hBS06 crossed the BBB to a similar extent in the BBB MPS (Figure 3B). The binding affinity of hBS01 to the iPS-BMECs was determined by evaluating the equilibrium dissociation constant (K_d). The iPS-BMECs were incubated with different concentrations of fluoresceinamine (FAM)-labeled starting pool (control) or hBS01 at 4 °C, and the fluorescence intensity was monitored by flow cytometry. As demonstrated in Supplementary Figure 6, the K_d of aptamer hBS01 for iPS-BMECs was 16.42 ± 1.97 nM, while that of starting pool was 81.02 ± 20.52 nM, indicating that hBS01 bound with higher affinity to the target cells. Given the higher BBB-penetrating capacity of hBS01, further analysis was restricted to this sequence.

To assess the robustness of MPS-SELEX methodology, we employed the human TfR binding aptamer, DW4,[28] which had been previously screened using traditional SELEX process against the purified TfR and subsequently modified, and

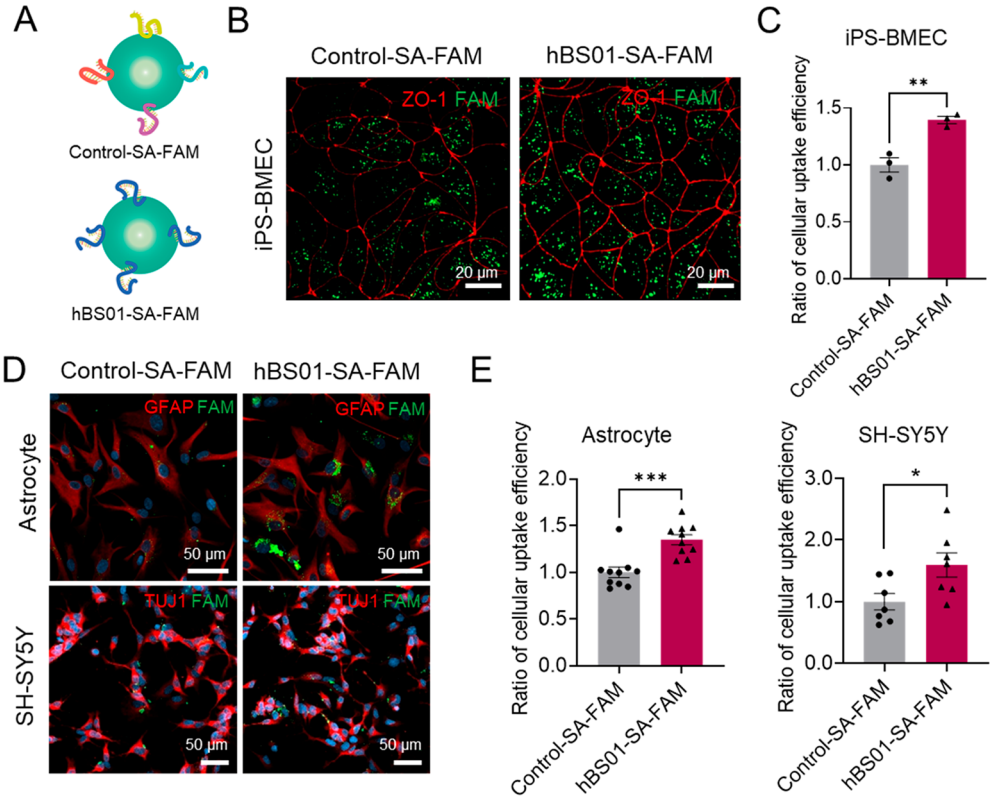

Figure 4. Cellular uptake efficiency of hBS01-SA-FAM in iPS-BMEC and brain cells. (A) Schematic illustration of FAM-conjugated streptavidin (SA) complexed with biotinylated starting pool ssDNA (control) or hBS01. (B) Confocal immunofluorescence micrographs of iPS-BMECs treated with Control-SA-FAM (green) or hBS01-SA-FAM (green) and labeled with ZO-1 (red). (C) Cellular uptake efficiency of hBS01-SA-FAM versus Control-SA-FAM in iPS-BMECs analyzed using ImageJ. For statistical analysis, an unpaired *t* test was performed. ($P < 0.01$). (D) Immunofluorescence images of astrocytes and neurons treated with Control-SA-FAM (green) or hBS01-SA-FAM (green). Human primary astrocytes and neuroblastoma SH-SY5Y cells were labeled with GFAP (red) and TUJ1 (red), respectively. (E) Cellular uptake efficiency of hBS01-SA-FAM versus Control-SA-FAM in astrocytes and neuroblastoma analyzed using ImageJ. For statistical analysis, an unpaired *t* test was performed. (*$P < 0.05$; ***$P < 0.001$).**

https://doi.org/10.1021/acsnano.2c11675
ACS Nano XXXX, XXX, XXX−XXX

compared its BBB penetration efficacy with that of hBS01 (Supplementary Figure 7). The results showed that DW4 does not demonstrate enhanced BBB penetration efficacy compared to the starting pool or scrambled DW4 (DW4sc)[28] and display a lower BBB influx rate when compared to hBS01 in our human BBB transwell model. This may be attributed to the inadequacy of the traditional screening method to discover BBB shuttle, which focuses solely on the internalization and binding affinity of aptamer to the target molecule, without considering its ability to penetrate through the cell.

To demonstrate the tissue-specific recognition capability of BBB01, we performed an endothelial permeability test to confirm whether the BBB-specific recognition of hBS01 is linked to tissue-specific extravasation efficiency. hBS01 ssDNA showed a 3-fold higher BBB penetration efficiency compared to the starting pool in the human BBB model (Figure 3C), but this trend was not observed in the human liver (Figure 3D), lung (Figure 3E), or umbilical cord endothelium (Figure 3F) transwell models. These data indicate that the recognized target ligand of hBS01 that leads to the exocytic pathway may be specifically expressed on the surface of BMECs. The enhanced targeting specificity of the selected aptamer was obtained using a single type of MPS in this study; however, introducing negative selection steps based on multiple tissue MPS may improve the cellular specificity by filtering out sequences binding to the unwanted endothelial cells.

hBS01 ssDNA Exhibits Higher Cellular Uptake in iPS-BMEC and Brain Cells. Streptavidin (SA), 60 kDa nanosized tetramer protein, has been used as a protein drug cargo model for targeted drug delivery applications because it allows site-specific binding of biotinylated ligands at each subunit through avidin-biotin interaction. To examine whether hBS01 could promote the intracellular uptake of the large cargo protein in target cells, we used FAM-labeled SA bound to either biotinylated hBS01 (hBS01-SA-FAM) or biotinylated starting pool (Control-SA-FAM). The stability of aptamer-SA nanocomplexes was confirmed in 37 °C up to 6 h (Supplementary Figure 8). The cellular uptake of hBS01-SA-FAM and Control-SA-FAM in iPS-BMECs were assessed using confocal microscopy imaging (Figure 4A) and flow cytometry analysis (Supplementary Figure 9). In agreement with the BBB permeability results, hBS01-SA-FAM exhibited significantly higher accumulation in iPS-BMECs in a human BBB MPS compared to Control-SA-FAM (Figure 4B,C). The flow cytometry results also support our claim that SA decorated with hBS01 displays significantly higher cellular uptake efficacy in iPS-BMECs compared to the control group (Supplementary Figure 9). However, when treated with the pulmonary or hepatic microvascular endothelium, or umbilical cord endothelium *in vitro*, differences in cellular uptake between hBS01-SA-FAM and Control-SA-FAM were not observed, which demonstrates the BBB-recognition of hBS01 (Supplementary Figure 10).

The hBS01 may efficiently bind to and internalize in human brain cells when transported across the BBB by recognizing a receptor expressed in both BMECs and brain cells. To explore this possibility, we further monitored the uptake of hBS01-SA-FAM versus Control-SA-FAM in human primary astrocytes, which accounts for the largest glial cell population in the CNS, and human brain neuroblastoma cell line (SH-SY5Y). Interestingly, we found that hBS01 significantly increased the cellular internalization of SA-FAM in human astrocytes and neuron cells (Figure 4D,E, and Supplementary Figure 9). It is assumed that the receptor recognized by hBS01 is commonly expressed in BMECs and brain cells at higher levels. Many studies have shown that receptors present in BMECs such as transferrin receptor,[29] insulin receptor,[30] and nicotinic acetylcholine receptors[31] are also observed in brain cells; therefore, it is not surprising to have multiple target specificity in the CNS as a BBB shuttle. Although this desired feature was obtained using a single type of MPS, more positive selection can be added to select aptamers with dual functionality. For example, using a neurovascular unit MPS with a linked human brain and BBB,[28,29] new sequences that possess BBB permeability and target specific neurons or glial cells may be discovered for highly controlled brain drug delivery.

To investigate the potential application of hBS01 as a tool for brain drug delivery, we assessed whether surface decoration of nanoparticles with hBS01 could improve the uptake and penetration of drug-loaded nanoparticles across the BBB. To achieve this, we utilized silica nanoparticles (SiNPs), which have been widely used as a safe and effective platform for drug delivery in clinical trials.[32] The COOH-functionalized SiNPs loaded with Rhodamine B isothiocyanate (RITC) dye as a model drug were conjugated with amine-modified aptamers. The conjugation of aptamers was confirmed successful, as evidenced by an increase in zeta potential to 40−50 mV. When observed by transmission electron microscopy, size of the particles was approximately 50−80 nm in diameter (Supplementary Figure 11).

We then treated iPS-BMECs with SiNPs conjugated with either the starting pool (control) or hBS01 and analyzed the particle uptake efficacy on iPS-BMECs by flow cytometry after 8 h of exposure. As shown in confocal fluorescence images, the hBS01-SiNP group had significantly higher uptake efficacy than the control-SiNP group, which is supported by flow cytometry analysis (Supplementary Figure 12). To further validate the penetration efficacy and simulate the drug delivery ability of hBS01-SiNPs to brain cancer cells, we coincubated human glioblastoma (U87) cells with aptamer-SiNPs that had penetrated the BBB. We observed substantially higher particle uptake in the hBS01-SiNP group in the fluorescent images, indicating that the hBS01 aptamer retains its functionality when conjugated to the nanoparticle (Supplementary Figure 12). These findings indicate that hBS01-SiNP holds great promise as a brain drug delivery system for the treatment of brain diseases by transporting therapeutics.

Involvement of Clathrin-Mediated Endocytosis in hBS01 Transcytosis. Next, we explored the mechanistic details of the intracellular transport pathway of hBS01 through BMEC. We revealed that hBS01 display enhanced specificity to BMEC and penetrate the BBB without affecting the cellular barrier; thus, we assumed that RMT is a mechanism for the transcellular transport of hBS01. Considering that endocytosis is a prerequisite step to vesicle-mediated transcellular transport across the BBB transcellular transport pathway, we selected two major endocytic pathways of BBB, clathrin-mediated endocytosis (CME) and caveolae-mediated endocytosis (CvME), as potential routes for hBS01 internalization. To determine which endocytic pathway is more involved in the transcellular transport of hBS01, the BBB transwell models were pretreated with inhibitors including chloropromazine and dynasore that target CME and genestin, which blocks CvME,[33] and the BBB permeability of hBS01 was analyzed. We found that the inhibition of CvME with genestin did not result in any change; however, when CME was inhibited, the transport of

https://doi.org/10.1021/acsnano.2c11675
ACS Nano XXXX, XXX, XXX−XXX

hBS01 was significantly decreased (Figure 5A). This trend was observed even when the BBB transwell was treated with a lower dose of inhibitors (Supplementary Figure 13). These data revealed that CME, but not CvME, is involved in hBS01 transport through the BBB. (Figure 5B)

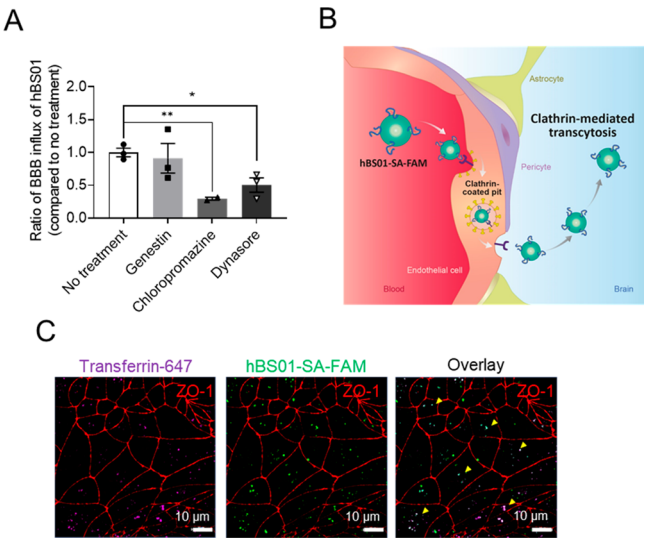

Figure 5. Cellular transcytosis mechanism of hBS01 in iPS-BMEC. (A) Fold change in BBB penetration efficacy when treated with two main endocytosis inhibitors. Genestrin for inhibition of caveolae-mediated endocytosis (CvME), and chlorpromazine and dynasore for inhibition of clathrin-mediated endocytosis (CME). For statistical analysis, an unpaired *t* test was performed (*P < 0.05; **P < 0.01). (B) Schematic illustration of transcytosis mechanism of hBS01-SA-FAM into brain. (C) Representative confocal fluorescence micrographs of iPS-BMECs labeled with ZO-1 showing colocalization of Transferrin-647 (magenta) as a marker of CME with hBS01-SA-FAM (green). Yellow arrows indicate regions of colocalization (white).

We further confirmed this finding by monitoring the intracellular localization of hBS01. We found that hBS01-SA-FAM colocalized with transferrin, confirming that intracellular trafficking of hBS01 is analogous to that of the transferrin receptor, which is known as CME[34] (Figure 5C). Taken together, these findings demonstrate that hBS01 is internalized into BMEC and successfully released to the basolateral membrane through a clathrin-dependent mechanism. It is well-known that CME is involved in most internalization processes mediated by approximately 20 different receptors in BMECs, including CME, CvME, and micropinocytosis.[35] Furthermore, several clinical trials of brain drugs formulated with BBB shuttles that specifically target CME have been conducted, including JR-141 fused with human anti-TfR[36] and AGT-181 complexed with human anti-insulin receptor.[37]

Once a vesicle is internalized, endosomal trafficking determines the efficacy of its transcellular transport across the BBB. The molecules that bind to the same receptor may show differential penetration in the BBB, depending on the binding affinity for the receptor at a lower pH (~5.5) in the intracellular vesicles.[38] Given that hBS01 bound to the receptor is internalized by CME vesicles and transported to the basolateral side of the BBB, hBS01 seems to avoid entrapment within intracellular vesicles efficiently in brain endothelial cells. Further investigation is needed to explore its putative receptors on BMECs, intracellular trafficking, and exocytotic release mechanism for a better understanding of the shuttling mechanism of hBS01.

Biodistribution and *Ex Vivo* Imaging of Mice Injected with hBS01. Having demonstrated the improved BBB penetration ability of hBS01, we validated the performance of hBS01 in an animal model. C57/BL6 mice were intravenously injected with either hBS01 or the starting pool for 1 h, and after perfusion with phosphate-buffered saline (PBS), brains were harvested to analyze the accumulated ssDNA using PCR (Figure 6A). In agreement with the *in vitro* results, the electrophoresis data showed that the signal of PCR products was approximately three times higher when mice were injected with hBS01 compared to the starting pool, indicating a greater brain targeting and BBB penetration capacity of hBS01 (Figure 6B,C).

We further monitored the shuttling capacity of hBS01 by injecting mice with either hBS01-SA labeled with Cy5.5 dye (hBS01-SA-Cy5.5) or Control-SA labeled with Cy5.5 (Control-SA-Cy5.5). Whole-body *in vivo* imaging system (IVIS) images showed that the mice administered hBS01-SA-Cy5.5 exhibited 2-fold higher fluorescence intensity in the brain compared to that of Control-SA-Cy5.5 at 30 min and 1 h postinjection (Figure 6D,E). To evaluate the biodistribution of nanocomplexes, major organs including the brain, liver, lungs, kidneys, spleen, and heart were collected following perfusion, and the fluorescence intensity in each organ was measured. Both formulations visibly accumulated in the liver and kidneys, which is common for SA nanocomplexes of comparable size, as reported previously[39] (Supplementary Figure 14). Nonetheless, in agreement with the *in vivo* distribution data, hBS01-SA-Cy5.5 showed brain accumulation significantly higher than that of Control-SA-Cy5.5 (Figure 6F,G).

The microscopic examination of the sectioned mouse brain also revealed the accumulation of hBS01-SA-Cy5.5 at the BBB and brain parenchyma near the BBB, which confirms that hBS01 allows the influx of molecules into the brain across the BBB *in vivo*. We also found that hBS01-SA-Cy5.5 was particularly accumulated high levels in the cortex, suggesting that the counterpart receptor of hBS01 may be enriched in the cortex region (Figure 6H). It shows the hBS01-SA-Cy5.5 complexes were mostly found outside the microvessel, while Control-SA-Cy5.5 complexes were mainly within microvessels. Furthermore, in the hippocampal region of the brain, a higher amount of hBS01-SA-Cy5.5 was also found compared to Control-SA-Cy5.5 (Figure 6I). These *in vivo* imaging and immunofluorescence data clearly demonstrate a significant enhancement of brain delivery of large protein cargo by hBS01. The optimization of sequences and chemical modifications of hBS01 are currently under further investigation to enhance serum stability and enhanced target specificity. It is also noteworthy that hBS01 was discovered and validated using human cells exhibits cross-species BBB shuttling ability, which implies that target recognition mechanism of hBS01 is not limited to human BBB.

Human MPS and *In Vivo*-SELEX Combined Approach. Even though hBS01 exhibited BBB shuttling capacity both in human BBB systems and mice *in vivo*, which is often an advantageous feature for broad applications as a BBB shuttle, we tested if the MPS and *in vivo* SELEX combined approach can select the aptamer with enhanced performance in mice *in vivo* while retaining the human BBB shuttling capacity. To investigate the possibility of human MPS and *in vivo* SELEX combined approach, we conducted two rounds of *in vivo*

https://doi.org/10.1021/acsnano.2c11675
ACS Nano XXXX, XXX, XXX−XXX

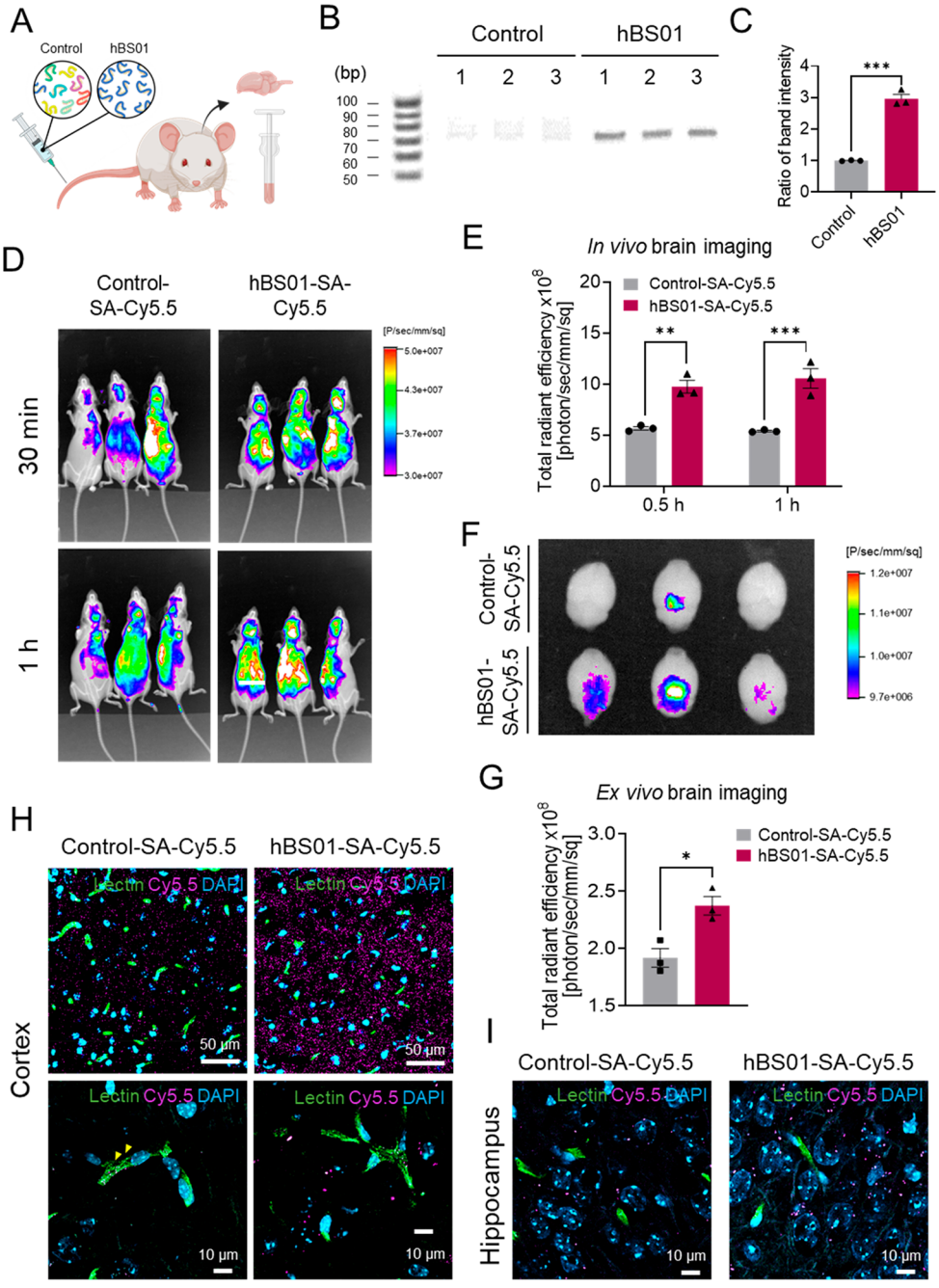

Figure 6. Biodistribution of hBS01 in mice. (A) Schematic of assessment process of hBS01 ssDNA accumulated in mouse brain. Perfused mouse brain was harvested following injection of the starting pool (control) or hBS01 and homogenized to harvest the brain-accumulated biotinylated aptamers. (B) Agarose gel electrophoresis to visualize the PCR amplified starting pool and hBS01 ssDNA obtained from mouse brain. (C) Quantitative analysis of PCR amplified hBS01 versus control by analyzing DNA band intensities using ImageJ. For statistical analysis, an unpaired *t* test was performed (*$P < 0.001$). (D) Dorsal view of mice depicting the fluorescence signal from Control-SA-Cy5.5 or hBS01-SA-Cy5.5 imaged by *in vivo* imaging system. (E) Total fluorescence radiant efficiency of the brain region. For statistical analysis, an unpaired *t* test was performed (**$P < 0.01$; ***$P < 0.001$). (F) Fluorescence signals from brains dissected from mice at 1 h post-treatment with Control-SA-Cy5.5 or hBS01-SA-Cy5.5 imaged by *in vivo* imaging system. (G) Total fluorescence radiant efficiency of the dissected brain. For statistical analysis, an unpaired *t* test was performed (*$P < 0.05$). Representative fluorescence microscopy images of (H) the cortex and (I) hippocampus area of the mouse brain. Brain microvessels are visualized using FITC-conjugated *Lycopersicon esculentum* lectin (green) and nuclei are stained with DAPI. Yellow arrows indicate the Control-SA-Cy5.5 found within the brain microvessels.**

SELEX by injecting an ssDNA pool obtained from fifth round of MPS-SELEX and compared the newly selected aptamer with hBS01. Following two rounds of *in vivo* SELEX, ssDNA was recovered from the mouse brain and sequenced using the Illumina deep sequencing platform (Figure 7A). The retrieved data identified four top sequences (hmBS01-hmBS04), as shown in Table S2, which were not top-ranked in the MPS-SELEX. When predicting their secondary structures using the M-fold web server,[27] hmBS02 and hmBS03 exhibited stem-loop structures (Figure 7B). Because a selected aptamer should retain its human BBB shuttling capacity, we first tested the BBB permeability of the top three aptamers using a human

https://doi.org/10.1021/acsnano.2c11675
ACS Nano XXXX, XXX, XXX−XXX

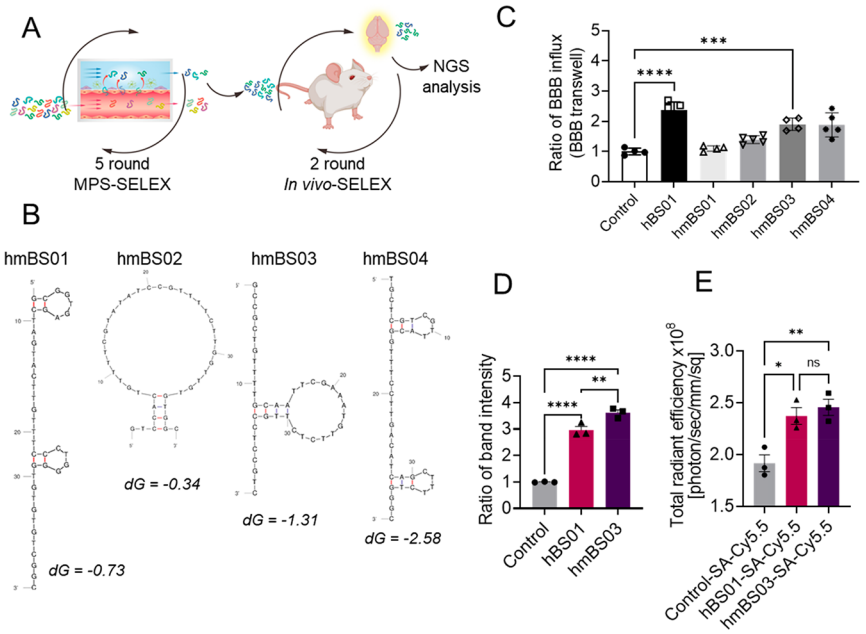

Figure 7. Human MPS and *in vivo*-SELEX combined approach. (A) The schematic diagram of human MPS-SELEX combined with mouse *in vivo*-SELEX. After five rounds of MPS-SELEX, the amplified aptamer pool was administered intravenously to mice for additional two round of *in vivo* SELEX. (B) The top four ranked aptamers from human MPS and *in vivo* combined SELEX (hmBS01-hmBS04). The secondary structure of selected aptamers simulated by M-fold software. *dG* = Gibbs free energy. (C) BBB penetration efficiencies of aptamers identified by combined SELEX approach versus starting pool (control) in the human BBB transwell model. For statistical analysis, an unpaired *t* test was performed (*$P < 0.001$; ****$P < 0.0001$). (D) Quantitative analysis of PCR amplified hBS01 and hmBS03 versus control by analyzing DNA band intensities using ImageJ. For statistical analysis, an unpaired *t* test was performed (**$P < 0.01$; ***$P < 0.001$; ****$P < 0.0001$). (E) Total fluorescence radiant efficiency of the brain region of mouse treated with Control-SA-Cy5.5, hBS01-SA-Cy5.5, or hmBS03-SA-Cy5.5. For statistical analysis, an unpaired *t* test was performed (*$P < 0.05$; **$P < 0.01$).**

BBB model. Among them, only hmBS03 displayed significantly higher BBB penetration compared to the starting pool (Figure 7C); thus, we selected hmBS03 as a candidate for further *in vitro* and *in vivo* assessments. The BBB penetration efficacy of hmBS03 was slightly lower than hBS01, however it showed a significantly higher value compared to control, which indicates that hmBS03 still retaining human BBB shuttling capacity. Interestingly, unlike hBS01-SA-FAM, which exhibited improved uptake in astrocytes and neurons, hmBS03-SA-FAM showed a higher uptake efficiency in astrocytes but not in neurons. Astrocytes and neurons share many common receptors such as dopamine receptor 1 and cannabinoid receptor type 1;[40] however, some receptors are reported to be expressed on astrocyte only.[41] Differential cell recognition of hBS01 and hmBS03 suggests that the recognized target receptors may differ between two aptamers (Supplementary Figure 15) and inclusion of *in vivo*-SELEX may enable the discovery of aptamer using different BBB penetration mechanism.

To test the performance of hmBS03 in an animal model, mice were treated with hmBS03 or the starting pool, and the amounts of aptamers in the brain at 1 h postinjection were analyzed using PCR. hmBS03 exhibited approximately 3.6 times higher accumulation in the brain compared to the starting pool, while hBS01 exhibited three times higher BBB permeability (Figure 7D and Supplementary Figure 16A). This result implies, while MPS-SELEX alone can screen for brain targeting aptamers, the inclusion of *in vivo*-SELEX may enable the selection of aptamers with higher brain specificity. *In vivo* distribution and brain *ex vivo* analysis also revealed significantly higher brain accumulation of hmBS03-SA-Cy5.5 versus Control-SA-Cy5.5. (Figure 7E and Supplementary Figure 16B–D) However, overall, the *in vivo* BBB shuttling performance of hmBS03 was not superior to that of hBS01, contrary to our expectations.

These findings show that human MPS and *in vivo*-combined SELEX can enrich new aptamers; however, only five rounds of MPS-SELEX can robustly enrich a functional BBB shuttle with BBB transport capacity in both humans and mice. This is possibly attributed to the insufficient number of rounds of *in vivo* selection, given that the past *in vivo* SELEX study performed 28 rounds of selection to identify the aptamer that functions in a live target. Further optimization of the combined SELEX strategy, including the number of rounds and the order of introduction of the *in vivo* SELEX procedure (before, in the middle, or after MPS-SELEX), will be required to discover enhanced BBB shuttle aptamers in the future.

CONCLUSIONS

Recent years have seen rapid development in the number and variety of MPS to mimic specific *in vivo* vascular environments; however, these MPSs have not been demonstrated as a screening platform to discover targeting moieties. In this study, we systemically investigated a SELEX approach using human MPS (MPS-SELEX), which offers a reliable platform for selecting BBB shuttle aptamers under physiological conditions. The human BBB MPS recapitulates the *in vivo* environment of the BBB, exhibiting physiologically relevant barrier functions and selective transcytosis of molecules, enabling the selection of aptamers with high BBB penetrating capacity among the small-sized ssDNA library. MPS-SELEX successfully identified a functional BBB shuttle aptamer, hBS01, which binds to the

https://doi.org/10.1021/acsnano.2c11675
ACS Nano XXXX, XXX, XXX−XXX

target expressed on the BMECs and efficiently penetrates the brain via the CME route. Moreover, hBS01 showed improved organ-specific shuttling capacity with enhanced cellular uptake and transmigration across the human BBB system but not in the lung or liver endothelium. We also found that hBS01 not only targets the BBB but also has the capacity to bind to human brain cells, suggesting that hBS01 may enable rapid and robust uptake in astrocytes and neurons when entering the brain. The high BBB shuttling capacity of hBS01 under physiological conditions was also demonstrated in mice *in vivo*, implying hBS01 has capacity to target brain while circulating through the blood. For enhanced brain targetability, human MPS-SELEX was combined with *in vivo*-SELEX to screen the aptamer, having BBB penetration capacity in both mice and human. The current study exploited only BBB MPS to screen BBB penetrating aptamer; however, this approach can be further improved by integrating multiple organ models such as liver and kidney MPS in an MPS-SELEX process, which can filter out aptamers targeting other organs. Our proposed approach might therefore be useful in the discovery of aptamer-based drug delivery approaches for a variety of brain pathologies and can be applied more broadly in various organ MPSs.

MATERIALS AND METHODS

Cell Culture. The human iPSC line IMR90-4 (WiCell Research Institute) was maintained according to the WiCell Feeder Independent Pluripotent Stem Cell Protocol provided by the WiCell Research Institute. Primary human astrocytes and pericytes (ScienCell) were maintained in the astrocyte medium (AM) and pericyte medium (PM), respectively. Human umbilical vascular endothelial cells (HUVECs) were purchased from Lonza and cultured in EGM-2 medium (Lonza). Primary human pulmonary microvascular endothelial cells (HPMEC) and human hepatic sinusoidal endothelial cells (HHSEC) were purchased from ScienCell and cultured in endothelial cell medium (ECM). Passages 3−6 of primary cells were used.

iPS-BMEC Differentiation. Differentiation was conducted using a previous method reported by Qian et al. with a minor modification.[21,22] IMR90-4 iPSC colonies were singularized using Accutase (Merck) at 70−80% confluence, and 1.7×10^5 cells were seeded on each well of a 6-well plate coated with Matrigel (Corning) with 10 μM Y27632 (Tocris Bioscience). The cells were maintained with TeSR-E8 (STEMCELL Technology) for 3 days. The culture medium was replaced with DeSR1 to induce differentiation into microvascular endothelial cells. DeSR1 was composed of DMEM/F12 (Gibco), 1× nonessential amino acids (100×) (Gibco), 0.5× GlutaMAX supplement (Thermo Fisher Scientific), and 0.1 mM β-mercaptoethanol (Gibco) supplemented with 6 μM CHIR-99021 (Sigma). Cells were fed daily with DeSR2: DeSR1 + B27 supplement (Thermo Fisher Scientific) without CHIR-99021 until the sixth day after the start of differentiation. Cells were maintained in endothelial cell medium (hECSR1) composed of human endothelial SFM (HESFM; Gibco) supplemented with 20 ng/mL of basic fibroblast growth factor (bFGF; Peprotech), 1× B-27 supplement, and 10 μM retinoic acid (RA; Sigma). Cells were harvested from 6-well plates and seeded on the blood channel of the chip at a density of 2.0×10^7 cells/mL. The medium was switched to hECSR2 (hECSR1 without bFGF or RA) and changed daily to maintain the BBB culture. From D0 to D9, the cells were cultured in a hypoxic incubator (Eppendorf Galaxy 48R) flushing with a 5% O_2-5% CO_2-N_2 balance and transferred to a regular CO_2 incubator.[21]

Fabrication of the MPS Device. The design of the BBB MPS was modified from the previous BBB-on-a-chip model reported by Park et al.[21] The MPS device was composed of an upper polydimethylsiloxane (PDMS) part, a lower PDMS part, a PET membrane sandwiched between two pieces of PDMS, and a cover glass supporting the device. The hollow microchannels were 2500 μm long and 1000 μm wide, and the top and bottom channels were 1000 and 200 μm high, respectively. The PET membrane was 10 μm thick, track-etched, and transparent. The membrane, which was a 2 μm perpendicular pore at a pore density of 1.6×10^6 pore/cm^2, was obtained from ipCELLCULTURE and processed as designed by laser cutting. PDMS was mixed in a 10:1 ratio of base to curing agent and then degassed in a desiccator (PolyLab). The mixed compound for the top channel was cast in an acrylic mold (Microfit), and the other for the bottom channel was cast in the SU-8 mold (Microfit). Mixed PDMS was cured at 80 °C for at least 6 h and trimmed as designed, and inlets and outlet holes were created with 1 mm biopsy punches. Each part of the PDMS was bonded to the PET membrane using the oxygen plasma treatment method reported by Tang and Lee.[23] The treatment was conducted under the following conditions: O_2 plasma at 80 W for 1 min, and O_2 gas flow from 50 sccm to 0.80 mbar. After treatment, to promote a bonding reaction, the PDMS parts were immersed in a 5% (3-aminopropyl)triethoxysilane solution (Sigma) and a PET membrane was immersed in a 1% (3-glycidyloxypropyl)-trimethoxysilane solution (Sigma) for 20 min at room temperature on a rotator. The parts and membranes were carefully dried using an air gun and aligned manually, following which they were pressed together and fixed with tongs. The completed device was stored in a 65 °C oven for over 2 days.

Reconstruction of the BBB MPS. The channel of the device was flushed with 70% EtOH and Dulbecco's phosphate buffered saline (DPBS; Welgene) twice and dried in a 65 °C oven. The device was subjected to oxygen plasma treatment under the following conditions: O_2 plasma at 80 W for 1 min, and O_2 gas flow of 50 sccm to 0.80 mbar. After the treatment, the channels of the device were immediately filled with poly-L-lysine (Merck) solution and incubated for 2 h at 37 °C. After washing with DPBS, BBB ECM solution (400 μg/mL collagen IV and 100 μg/mL fibronectin) was filled, and the device was incubated for at least 12 h at 37 °C. On the day of cell seeding, the channels were washed with the pericyte medium (ScienCell). Astrocytes and pericytes were seeded on the brain channel of the chip at a density of 0.1×10^6 cells/mL and 0.05×10^6 cells/mL, respectively. Two hours after seeding, entire channels of the MPS device were washed with hECSR1. The iPS-BMECs were seeded on the blood channel of the MPS device at a density of 2×10^7 cells/mL, and the MPS device was flipped immediately to allow iPS-BMECs to attach to the ECM-coated PET membrane. After 6 h of incubation in a hypoxic chamber, the device was flipped back to its original orientation, and hECSR1 was slightly infused to remove unattached cells. The device was incubated in a hypoxic chamber for another 18 h, and the BBB MPS was subsequently fed fresh hECSR2 and transferred to a regular incubator. The BBB transwell model was established by seeding iPS-BMECs on a 24-well transwell insert with 0.4 μm pore PET (Corning) at a density of 3.3×10^5 cells cocultured with a mixture of astrocytes (1.16×10^4 cells/well) and pericytes (0.58×10^4 cells/well) in the basal chamber.

Immunocytochemistry and Confocal Imaging. On the third day after culture, the BBB MPS was fixed with 4% paraformaldehyde (PFA) for 15 min and permeabilized with 0.1% Triton X-100 (Sigma) for 10 min at room temperature. Blocking was performed for 30 min in 10% goat serum in 0.1% Triton X-100. Primary antibodies were treated by infusing the antibody solution through the channels and incubating overnight at 4 °C. The inlets and outlets were blocked using pipet tips to prevent drying. After washing three times, the cells were incubated with secondary antibodies for 1 h at room temperature in the dark. The following antibodies were used: Claudin-5 (mouse monoclonal; Invitrogen; 352588), Occludin (mouse monoclonal; Invitrogen; 33-1500), ZO-1 (mouse monoclonal; Invitrogen; 339194), GLUT-1 (mouse monoclonal; Abcam; ab40084), Fluor-488 (donkey polyclonal; Abcam; ab150109), and Alexa Fluor-647 (donkey polyclonal; Abcam; ab150063). Nuclei were counterstained with DAPI (Sigma). Confocal imaging was carried out using a Zeiss LSM980 with multiplex mode.

Single-Strand DNA Library and Blocking Sequences. The ssDNA library, 5′-AAGTAAGCAGCACAGAGGTCAGATG-N40-

https://doi.org/10.1021/acsnano.2c11675
ACS Nano XXXX, XXX, XXX−XXX

CCTATGCGTGCTACCGTGAA-3′, was synthesized based on the method previously reported by Ouellet et al.,[26] with some modifications. It was composed of 40 random nucleotides having 4^{40} diversity and primer hybridization sites at both ends. Complementary sequences against both primers named 5′-block (5′-CATCTGACCTCTGTGCTGCTTACTT-3) and 3′-block (5′-biotin-TTCACGGTAGCACGCATAGG-3′) were synthesized to block 5′ and 3′ primer site, respectively. The 3′-block was biotinylated to efficiently isolate aptamers using a biotin-avidin reaction. The primers and ssDNA library were synthesized and purified using high-performance liquid chromatography (Bioneer).

MPS-SELEX. For the first MPS-SELEX round, 10 nmol of ssDNA library and 5′-block and 3′-block blocking sequences were diluted in 150 μL of HESFM. The ssDNA library was denatured by heating at 95 °C for 5 min and cooled at room temperature for 10 min to allow each DNA sequence to form a stable secondary structure. The starting pool was dosed into the blood channel of the BBB MPS connected to a syringe pump, and a cycle of withdrawal for 1.5 h and infusion for 1.5 h at 100 μL/h was repeated twice for 6 h. We collected apical and basal effluents and added 350 μL of EtOH to precipitate the recovered DNA. Briefly, effluents were treated with 1/10 volume of 3 M sodium acetate and two volumes of EtOH and stored at −20 °C overnight. Next, the mixture was centrifuged at 15,000 rpm for 20 min and rinsed with 70% EtOH. The precipitated DNA was resuspended in distilled water, and the concentration of ssDNA was measured using NanoDrop (Thermo Fisher Scientific) to monitor the enrichment of BBB-permeable aptamers following each round of MPS-SELEX. The recovered DNA was amplified using PCR and used in the next round. To confirm the barrier function of the BBB during MPS-SELEX, 0.1 mg/mL of lucifer yellow was used as a fluorescent tracer and quantified by measuring fluorescence intensity at 420/520 nm.

Analysis of Aptamer Sequences and Secondary Structures. To analyze the BBB-penetrating aptamer sequence, the ssDNA library pool obtained from the final round of SELEX was amplified using symmetric PCR. The sequences of the amplified double-stranded DNAs (dsDNA) were determined by next-generation sequencing (NGS) using the TruSeq Nano DNA Kit on an illumine platform (Macrogen). The secondary structures of the ssDNA aptamers were predicted using the M-fold-free software.[27]

Conjugation of Aptamer and Streptavidin Particle. Streptavidin (Thermo Fisher Scientific) was labeled with the fluorescent dye Cy5.5 NHS ester or FAM NHS ester at a 1:30 (w/w) ratio. The mixture was incubated at room temperature for 4 h. A fluorescent-labeled streptavidin solution was filtered using a Microcon-30 kDa Centrifugal Filter (Merck) to remove the free dye. The candidate aptamer and fluorescent-labeled streptavidin were mixed at a 2.66:1 molar ratio on a rotator at room temperature for 1 h.

Assessment of BBB Penetration and Cellular Uptake of ssDNA. The BBB penetration efficiencies of the BBB shuttle candidates were assessed using the BBB MPS and BBB transwell system. In the BBB MPS, 2.6 μM ssDNA sequences (Bioneer) were fluxed into the blood channel at a flow rate of 100 μL/h. Effluents from the blood and brain channels were collected for 6 h, and EtOH precipitation was conducted to purify DNA following the protocol mentioned above. The concentration of the purified ssDNA was determined using NanoDrop to evaluate the rate of flux of the aptamer across the BBB. The rate of flux (w/w) was calculated by dividing the amount of aptamer output through the brain channel by the amount of aptamer input through the blood channel.

On the other hand, in the BBB transwell system, an apical chamber was treated with 0.4 nmol aptamers on a shaker, and the media was collected every 15 min from the basal chamber for 1 h. The concentration of the purified ssDNA was determined using NanoDrop to evaluate the rate of flux of the aptamer across the cellular interface. For measurement of BBB penetrated aptamer concentration, Qubit quantitative detection was performed. Twenty μL of collected sample was added into a 180 μL of Qubit ssDNA working solution (1:200 ratio of reagent), and the mixture was incubated at room temperature for 2 min. Concentrations of ssDNA were measured using a Qubit 3.0 Fluorometer. To examine the tissue-recognition ability of the hBS01 aptamer *in vitro*, the rate of flux of hBS01 in the BBB transwell mode was compared with that in the transwell with lung, liver, and umbilical cord endothelium. To establish the lung, liver, and umbilical cord endothelium models, HPMECs (ScienCell), HHSECs (ScienCell), and HUVEC (Lonza) were seeded at a density of 3×10^4 cells in the apical chamber of a 24-well transwell (Corning), respectively, and cultured for 2 days to form a confluent monolayer. To observe the cellular uptake of aptamer, the transwell models were treated with 0.04 nmol of hBS01-SA-FAM or Control-SA-FAM for 1 h. The endothelial cells were subsequently washed three times with PBS, fixed using 4% PFA, and stained with DAPI. Confocal microscopy analysis was performed using a confocal microscope (ZEISS LSM 980), and the number of internalized complexes was analyzed using ImageJ software.

Aptamer Stability Analysis. To confirm the stability of primer site hybridization during screening, a mixture of 1 μM of library aptamer and 3′ and 5′ ends was prepared in 100 μL of HESFM. The mixture was then heated at 95 °C for 5 min, followed by a 10 min rest at room temperature. Fifteen μL of the sample was taken and stored at −80 °C, while the remainder was incubated at 37 °C. This process was repeated every 3 h until the 9 h time point, with the final sample being taken after 24 h. The stability of those five samples was then assessed using 4% agarose gel electrophoresis. To assess the stability of Control-SA-FAM and hBS01-SA-FAM, 0.05 nmol of aptamers was conjugated with SA-FAM and incubated in either HESFM or HESFM with 10% FBS at 37 °C. Samples were taken at each time point and analyzed using 4% agarose gel electrophoresis.

Flow Cytometry Analysis. Human primary astrocytes and SH-SY5Y cells were seeded at the density of 1×10^5 cell per well in 12-well plate. At a confluency of 80%, both cells were treated with 0.5 nmol of Control-SA-FAM or hBS01-SA-FAM for 2 h. The iPS-BMECs cocultured with astrocytes and pericytes in a transwell system were similarly treated with 0.5 nmol of Control-SA-FAM or hBS01-SA-FAM for 30 min. Cells were washed with DPBS and detached using 0.25% trypsin-EDTA for astrocytes and SH-SY5Y and Accutase (Merck) for iPS-BMECs. The cell samples were prepared by centrifugation at 500*g* for 4 min at 4 °C, washed twice, resuspended in 200 μL of DPBS for flow cytometric analysis.

The affinity of aptamers to target iPS-BMECs was quantitatively assessed by measuring the K_d. The K_d values were calculated by nonlinear regression method for one-site binding using Graph-pad Prism. The iPS-BMECs were incubated with different concentrations (0−1000 nM) of control and hBS01 labeled with FAM at 5′ block primer at 4 °C for 1 h in the dark. After washing with PBS, fluorescence intensity was analyzed using flow cytometry. The K_d value was calculated by measuring the mean fluorescence intensity of aptamers by different aptamer concentrations using the following equation: $Y = B_{max} \times X/(K_d + X)$. The binding affinity assay was performed three times independently.

Investigation of Aptamer Internalization Mechanism. The endocytic pathway of the hBS01 aptamer was investigated using a human BBB transwell model by monitoring the rate of flux of hBS01 across the brain endothelium in the presence of endocytosis inhibitors. The BBB transwell model was pretreated with 50 μM genestin (Sigma), which inhibits CvME, 50 μM chlorpromazine (Sigma), or 80 μM dynasore (Sigma) to block CME. Thirty min after pretreatment with inhibitors, iPS-BMECs were treated with 0.4 nmol of hBS01 in the apical chamber and incubated on a shaker for 1 h. To monitor the barrier integrity, 0.1 mg/mL of lucifer yellow was dosed simultaneously. The media was collected from the basal chamber, and the concentration of ssDNA was measured to analyze the ratio of BBB-penetrated aptamers. To investigate the involvement of CME, a BBB transwell model was coincubated with hBS01-SA-FAM and Alexa Fluor 647-conjugated transferrin (Thermo Fisher Scientific) as a marker of CME on a shaker for 1 h. Subsequently, cells were washed with PBS and fixed with 4% PFA for 10 min. Fluorescence microscopy was performed on a ZEISS LSM 980, and colocalization of hBS01-SA-Cy5.5 and Alexa Fluor 647-conjugated transferrin was analyzed using ImageJ.

https://doi.org/10.1021/acsnano.2c11675
ACS Nano XXXX, XXX, XXX−XXX

Intravenous Injection into C57BL/6 Mouse and Brain Collection. Aptamer injection and brain collection were conducted by a contract research organization (NDIC). 100 μL of the aptamer at a 20 μM concentration was injected through the tail vein into a C57BL/6 mouse. After 1 h, blood was removed through heart perfusion, and the brain was extracted. The extracted brain was homogenized in RIPA buffer and then centrifuged at 4 °C at 15000 rpm for 5 min. The supernatant was transferred to a new tube, and streptavidin magnetic beads (NEB) were added and shaken at room temperature for 10 min. A tube was inserted into the magnetic stand to induce streptavidin magnetic beads to adhere to the tube wall, washed twice with DW, and beads were collected with 20 μL of DW. The collected beads were used as PCR templates, and PCR was performed using pfu DNA polymerase (Biofact).

Biodistribution of Aptamer-Decorated SA Complexes on *In Vivo* and *Ex Vivo* Model. BALB/c nude 7 week-old female mice (Orient Bio) and BALB/c 7 week-old female mice (Orient Bio) were used for *in vivo* live imaging and *ex vivo* imaging. An aptamer conjugated with streptavidin-Cy5.5 (5 nmol) was systemically administered to the mouse via tail vein injection. For *in vivo* live imaging, mice were anesthetized with 2% isoflurane and positioned facing up at 30 min and 1 h time points. *In vivo* images were captured using In-Vivo Xtreme II (Bruker), and the radiant efficiency from the region of interest (ROI) placed over the head was quantified using In-Vivo Xtreme II imaging software. The shape of skull of each mouse obtained from an X-ray image was used to determine the ROI of head. For *ex vivo* imaging, mice were anesthetized with 2% isoflurane at 1 h after injection. Cardiac perfusion was conducted sequentially using DMEM, PBS with 0.01% Tween20, and DMEM to remove unpenetrated aptamer particles from the vessel. Subsequently, the brains were isolated and placed on a square dish for fluorescence imaging with an In-Vivo Xtreme II (Bruker). Radiance efficiency within a ROI was quantified using In-Vivo Xtreme II imaging software. All animal experiments were conducted in accordance with the Institutional Animal Care and Use Committee (IACUC) guidelines (UNISTIACUC-22-06).

Tissue Section Imaging. Dye-conjugated SA bound to the biotinylated aptamers (5 nmol) were intravenously injected and circulated for 1 h. To visualize the microvessels, 50 μg of FITC-conjugated Lycopersicon (Tomato) esculentum lectin was administered 30 min before perfusion. Mouse brains were perfused with DPBS for 4 min and fixed with neutral buffered formalin (NBF). Brains were harvested, incubated overnight in NBF at room temperature for additional fixation, and sequentially incubated in 10%, 20%, and 30% sucrose solutions overnight. For tissue block preparation, brains were then embedded in optimum cutting temperature compound (OCT) and frozen at −20 °C. Brain tissues were sectioned at 10 μm thickness and mounted using Vectershield VECTASHIELD (Vector Laboratories) for observation.

Preparation and Characterization of Aptamer Conjugated Silica Nanoparticles. Fluorescent Fe3O4@SiO2 nanoparticle containing Rhodamine B isothiocyanate (RITC) dye was purchased from Biterials Co. Ltd. To conjugate the candidate aptamer, 20 μL of COOH-functionalized Fe_3O_4@SiO_2 nanoparticles in 2 mg/mL of borate buffer solution was sequentially treated with 2 mg of sulfo-NHS, 1.1 μL of EDC, and 10 μL of candidate aptamer (1000 pmol/μL) under continuous shaking (700 rpm) at room temperature for 6 h. After the process, the resulting mixture was purified using centrifuge and washed with PBS. The final product was resuspended in PBS and stored in the dark at 4 °C until use. To conduct TEM observation, 10 μg of SiNPs was dispersed in 100 μL of ethanol, and then 10 μL of the solution was dropped onto a carbon grid. TEM imaging was carried out using a Tecnai G2 F20 X-Twin instrument (FEI). Confirmation of aptamer conjugation with the nanoparticle was validated through zeta-potential analysis performed by Zetasizer Nano ZS (Malvern Instruments). Samples were diluted to 0.02 mg/mL in distilled water and sonicated before the measurement. Measurements were performed at 25 °C, and the viscosity and refractive index of the solutions were 0.8872 cP and 1.33, respectively.

Statistical analysis. All data are presented as mean (±SEM). The statistical analyses were performed using unpaired *t* tests in Prism (GraphPad). The *p*-values <0.05 were considered significant (*P < 0.05, **P < 0.01, ***P < 0.001, and ****P < 0.0001).

ASSOCIATED CONTENT

Supporting Information

The Supporting Information is available free of charge at https://pubs.acs.org/doi/10.1021/acsnano.2c11675.

Characterization of BBB MPS, cellular uptake efficiency and biodistribution of hBS01 and hmBS03 (PDF)

AUTHOR INFORMATION

Corresponding Authors

Jinmyoung Joo − *Department of Biomedical Engineering, College of Information and Biotechnology, Ulsan National Institute of Science and Technology (UNIST), Ulsan, Republic of Korea 44919;* orcid.org/0000-0003-1574-9842; Email: jjoo@unist.ac.kr

Tae-Eun Park − *Department of Biomedical Engineering, College of Information and Biotechnology, Ulsan National Institute of Science and Technology (UNIST), Ulsan, Republic of Korea 44919;* orcid.org/0000-0003-3979-5405; Email: tepark@unist.ac.kr

Authors

Jeong-Won Choi − *Department of Biomedical Engineering, College of Information and Biotechnology, Ulsan National Institute of Science and Technology (UNIST), Ulsan, Republic of Korea 44919*

Minwook Seo − *Department of Biomedical Engineering, College of Information and Biotechnology, Ulsan National Institute of Science and Technology (UNIST), Ulsan, Republic of Korea 44919*

Kyunghwan Kim − *Department of Chemistry, College of Natural Sciences, Ulsan National Institute of Science and Technology (UNIST), Ulsan, Republic of Korea 44919*

A-Ru Kim − *Nexmos, Inc., Yongin-si, Gyeonggi-do, Republic of Korea 16827*

Hakmin Lee − *Nexmos, Inc., Yongin-si, Gyeonggi-do, Republic of Korea 16827*

Hyung-Seok Kim − *Department of Forensic Medicine, Chonnam National University, Gwangju, Republic of Korea 61186*

Chun Gwon Park − *Department of Biomedical Engineering, SKKU Institute for Convergence, Sungkyunkwan University (SKKU), Suwon, Gyeonggi, Republic of Korea 16419; Department of Intelligent Precision Healthcare Convergence, SKKU Institute for Convergence, Sungkyunkwan University (SKKU), Suwon, Gyeonggi, Republic of Korea 16419*

Seung Woo Cho − *Department of Biomedical Engineering, College of Information and Biotechnology, Ulsan National Institute of Science and Technology (UNIST), Ulsan, Republic of Korea 44919*

Joo H. Kang − *Department of Biomedical Engineering, College of Information and Biotechnology, Ulsan National Institute of Science and Technology (UNIST), Ulsan, Republic of Korea 44919;* orcid.org/0000-0001-9636-3209

Complete contact information is available at: https://pubs.acs.org/10.1021/acsnano.2c11675

Author Contributions

$^{\nabla}$These authors contributed to this work equally.

https://doi.org/10.1021/acsnano.2c11675
ACS Nano XXXX, XXX, XXX−XXX

Funding

This work was supported by a National Research Foundation of Korea (NRF) grant (NRF- 2020R1C1C1014753 and 2021R1A4A3030597), the Korea Health Technology R&D Project (HU20C0094), the Korean Fund for Regenerative Medicine (KFRM) (RS-2022-00070678), and UNIST research grant (1.230039.01).

Notes

The authors declare no competing financial interest.

REFERENCES

(1) Daneman, R.; Prat, A. The blood–brain barrier. *Cold Spring Harbor perspectives in biology* **2015**, *7* (1), a020412.
(2) Pandit, R.; Chen, L.; Götz, J. The blood-brain barrier: Physiology and strategies for drug delivery. *Advanced drug delivery reviews* **2020**, *165*, 1–14.
(3) Zhang, W.; Mehta, A.; Tong, Z.; Esser, L.; Voelcker, N. H. Development of Polymeric Nanoparticles for Blood-Brain Barrier Transfer-Strategies and Challenges. *Adv. Sci. (Weinh)* **2021**, *8* (10), 2003937.
(4) Friden, P. M.; Walus, L. R.; Musso, G. F.; Taylor, M. A.; Malfroy, B.; Starzyk, R. M. Anti-transferrin receptor antibody and antibody-drug conjugates cross the blood-brain barrier. *Proc. Natl. Acad. Sci. U. S. A.* **1991**, *88* (11), 4771–4775.
(5) Ulbrich, K.; Hekmatara, T.; Herbert, E.; Kreuter, J. Transferrin- and transferrin-receptor-antibody-modified nanoparticles enable drug delivery across the blood–brain barrier (BBB). *Eur. J. Pharm. Biopharm.* **2009**, *71* (2), 251–256.
(6) Demeule, M.; Currie, J. C.; Bertrand, Y.; Ché, C.; Nguyen, T.; Régina, A.; Gabathuler, R.; Castaigne, J. P.; Béliveau, R. Involvement of the low-density lipoprotein receptor-related protein in the transcytosis of the brain delivery vector Angiopep-2. *Journal of neurochemistry* **2008**, *106* (4), 1534–1544.
(7) Lee, J. H.; Engler, J. A.; Collawn, J. F.; Moore, B. A. Receptor mediated uptake of peptides that bind the human transferrin receptor. *European journal of biochemistry* **2001**, *268* (7), 2004–2012.
(8) Li, J.; Feng, L.; Fan, L.; Zha, Y.; Guo, L.; Zhang, Q.; Chen, J.; Pang, Z.; Wang, Y.; Jiang, X.; et al. Targeting the brain with PEG–PLGA nanoparticles modified with phage-displayed peptides. *Biomaterials* **2011**, *32* (21), 4943–4950.
(9) Xiong, X.; Liu, H.; Zhao, Z.; Altman, M. B.; Lopez-Colon, D.; Yang, C. J.; Chang, L. J.; Liu, C.; Tan, W. DNA aptamer-mediated cell targeting. *Angew. Chem.* **2013**, *125* (5), 1512–1516.
(10) Macdonald, J.; Henri, J.; Goodman, L.; Xiang, D.; Duan, W.; Shigdar, S. Development of a Bifunctional Aptamer Targeting the Transferrin Receptor and Epithelial Cell Adhesion Molecule (EpCAM) for the Treatment of Brain Cancer Metastases. *ACS Chem. Neurosci.* **2017**, *8* (4), 777–784.
(11) Di Caprio, N.; Bellas, E. Collagen stiffness and architecture regulate fibrotic gene expression in engineered adipose tissue. *Adv. Biosyst* **2020**, *4* (6), 1900286.
(12) Sola, M.; Menon, A. P.; Moreno, B.; Meraviglia-Crivelli, D.; Soldevilla, M. M.; Carton-Garcia, F.; Pastor, F. Aptamers Against Live Targets: Is In Vivo SELEX Finally Coming to the Edge? *Mol. Ther Nucleic Acids* **2020**, *21*, 192–204.
(13) Cheng, C.; Chen, Y. H.; Lennox, K. A.; Behlke, M. A.; Davidson, B. L. In vivo SELEX for Identification of Brain-penetrating Aptamers. *Mol. Ther Nucleic Acids* **2013**, *2*, e67.
(14) Tuerk, C.; Gold, L. Systematic evolution of ligands by exponential enrichment: RNA ligands to bacteriophage T4 DNA polymerase. *Science* **1990**, *249* (4968), 505–510.
(15) Ellington, A. D.; Szostak, J. W. In vitro selection of RNA molecules that bind specific ligands. *nature* **1990**, *346* (6287), 818–822.
(16) Darmostuk, M.; Rimpelova, S.; Gbelcova, H.; Ruml, T. Current approaches in SELEX: An update to aptamer selection technology. *Biotechnology advances* **2015**, *33* (6), 1141–1161.
(17) Wang, T.; Chen, C.; Larcher, L. M.; Barrero, R. A.; Veedu, R. N. Three decades of nucleic acid aptamer technologies: Lessons learned, progress and opportunities on aptamer development. *Biotechnol Adv.* **2019**, *37* (1), 28–50.
(18) Zhang, W.; Liu, Q. Y.; Haqqani, A. S.; Leclerc, S.; Liu, Z.; Fauteux, F.; Baumann, E.; Delaney, C. E.; Ly, D.; Star, A. T.; et al. Differential expression of receptors mediating receptor-mediated transcytosis (RMT) in brain microvessels, brain parenchyma and peripheral tissues of the mouse and the human. *Fluids Barriers CNS* **2020**, *17* (1), 47.
(19) Dua, P.; Kang, S.; Shin, H. S.; Kim, S.; Lee, D. K. Cell-SELEX-Based Identification of a Human and Mouse Cross-Reactive Endothelial Cell-Internalizing Aptamer. *Nucleic Acid Ther* **2018**, *28* (4), 262–271.
(20) Dua, P.; Kang, S.; Shin, H.-S.; Kim, S.; Lee, D.-k. Cell-SELEX-based identification of a human and mouse cross-reactive endothelial cell-internalizing aptamer. *Nucleic acid therapeutics* **2018**, *28* (4), 262–271.
(21) Park, T. E.; Mustafaoglu, N.; Herland, A.; Hasselkus, R.; Mannix, R.; FitzGerald, E. A.; Prantil-Baun, R.; Watters, A.; Henry, O.; Benz, M.; et al. Hypoxia-enhanced Blood-Brain Barrier Chip recapitulates human barrier function and shuttling of drugs and antibodies. *Nat. Commun.* **2019**, *10* (1), 2621.
(22) Qian, T.; Maguire, S. E.; Canfield, S. G.; Bao, X.; Olson, W. R.; Shusta, E. V.; Palecek, S. P. Directed differentiation of human pluripotent stem cells to blood-brain barrier endothelial cells. *Science advances* **2017**, *3* (11), e1701679.
(23) Tang, L.; Lee, N. Y. A facile route for irreversible bonding of plastic-PDMS hybrid microdevices at room temperature. *Lab Chip* **2010**, *10*, 1274–1280.
(24) Lippmann, E. S.; Al-Ahmad, A.; Azarin, S. M.; Palecek, S. P.; Shusta, E. V. A retinoic acid-enhanced, multicellular human blood-brain barrier model derived from stem cell sources. *Sci. Rep.* **2014**, *4* (1), 1–10.
(25) Shi, L.; Zeng, M.; Sun, Y.; Fu, B. M. Quantification of blood-brain barrier solute permeability and brain transport by multiphoton microscopy. *J. Biomech Eng.* **2014**, *136* (3), 031005.
(26) Ouellet, E.; Lagally, E. T.; Cheung, K. C.; Haynes, C. A. A simple method for eliminating fixed-region interference of aptamer binding during SELEX. *Biotechnol. Bioeng.* **2014**, *111* (11), 2265–2279.
(27) Zuker, M. Mfold web server for nucleic acid folding and hybridization prediction. *Nucleic Acids Res.* **2003**, *31* (13), 3406–3415.
(28) Porciani, D.; Signore, G.; Marchetti, L.; Mereghetti, P.; Nifosì, R.; Beltram, F. Two interconvertible folds modulate the activity of a DNA aptamer against transferrin receptor. *Molecular Therapy-Nucleic Acids* **2014**, *3*, e144.
(29) Qian, Z. M.; To, Y.; Tang, P. L.; Feng, Y. M. Transferrin receptors on the plasma membrane of cultured rat astrocytes. *Exp Brain Res.* **1999**, *129* (3), 473–476.
(30) Masters, B. A.; Shemer, J.; Judkins, J. H.; Clarke, D. W.; Le Roith, D.; Raizada, M. K. Insulin receptors and insulin action in dissociated brain cells. *Brain Res.* **1987**, *417* (2), 247–256.
(31) Shen, J.-x.; Yakel, J. L. Functional α7 nicotinic ACh receptors on astrocytes in rat hippocampal CA1 slices. *Journal of Molecular Neuroscience* **2012**, *48* (1), 14–21.
(32) Janjua, T. I.; Cao, Y.; Yu, C.; Popat, A. Clinical translation of silica nanoparticles. *Nature Reviews Materials* **2021**, *6* (12), 1072–1074.
(33) Ariful Islam, M.; Park, T.-E.; Firdous, J.; Li, H.-S.; Jimenez, Z.; Lim, M.; Choi, J.-W.; Yun, C.-H.; Cho, C.-S. Essential cues of engineered polymeric materials regulating gene transfer pathways. *Prog. Mater. Sci.* **2022**, *128*, 100961.
(34) Morad, G.; Carman, C. V.; Hagedorn, E. J.; Perlin, J. R.; Zon, L. I.; Mustafaoglu, N.; Park, T.-E.; Ingber, D. E.; Daisy, C. C.; Moses, M. A. Tumor-derived extracellular vesicles breach the intact blood–brain barrier via transcytosis. *ACS Nano* **2019**, *13* (12), 13853–13865.

https://doi.org/10.1021/acsnano.2c11675
ACS Nano XXXX, XXX, XXX–XXX

(35) Pulgar, V. M. Transcytosis to Cross the Blood Brain Barrier, New Advancements and Challenges. *Front Neurosci* **2019**, *12*, 1019.
(36) Sonoda, H.; Morimoto, H.; Yoden, E.; Koshimura, Y.; Kinoshita, M.; Golovina, G.; Takagi, H.; Yamamoto, R.; Minami, K.; Mizoguchi, A.; et al. A Blood-Brain-Barrier-Penetrating Anti-human Transferrin Receptor Antibody Fusion Protein for Neuronopathic Mucopolysaccharidosis II. *Mol. Ther* **2018**, *26* (5), 1366−1374.
(37) Boado, R. J.; Hui, E. K.; Lu, J. Z.; Pardridge, W. M. AGT-181: expression in CHO cells and pharmacokinetics, safety, and plasma iduronidase enzyme activity in Rhesus monkeys. *J. Biotechnol.* **2009**, *144* (2), 135−141.
(38) Sade, H.; Baumgartner, C.; Hugenmatter, A.; Moessner, E.; Freskgård, P.-O.; Niewoehner, J. A human blood-brain barrier transcytosis assay reveals antibody transcytosis influenced by pH-dependent receptor binding. *PLoS One* **2014**, *9* (4), e96340.
(39) Jain, A.; Barve, A.; Zhao, Z.; Jin, W.; Cheng, K. Comparison of avidin, neutravidin, and streptavidin as nanocarriers for efficient siRNA delivery. *Mol. Pharmaceutics* **2017**, *14* (5), 1517−1527.
(40) Shan, L.; Zhang, T.; Fan, K.; Cai, W.; Liu, H. Astrocyte-neuron signaling in synaptogenesis. *Frontiers in Cell and Developmental Biology* **2021**, *9*, 1786.
(41) Kimelberg, H. K.; Nedergaard, M. Functions of astrocytes and their potential as therapeutic targets. *Neurotherapeutics* **2010**, *7* (4), 338−353.

https://doi.org/10.1021/acsnano.2c11675
ACS Nano XXXX, XXX, XXX−XXX